Engineering Structures 309 (2024) 118055

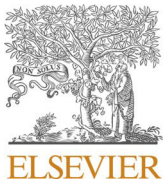

Contents lists available at ScienceDirect

Engineering Structures

journal homepage: www.elsevier.com/locate/engstruct

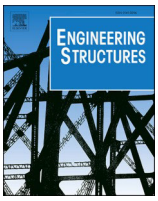

A corner protrusion strategy for the aerodynamic response mitigation of tall buildings with the aim of using non-structural components

Wei-Ting Lu [a], Brian M. Phillips [a,*], Zhaoshuo Jiang [b]

[a] Department of Civil and Coastal Engineering, University of Florida, Gainesville, United States
[b] Department of Civil and Environmental Engineering, San Francisco State University, San Francisco, United States

ARTICLE INFO

Keywords:
Wind tunnel testing
High-rise building
Aerodynamic strategy
Nonstructural component
Façade
Side protrusion

ABSTRACT

Side protrusion, i.e., the addition of material on the side of a tall building, has been demonstrated as an effective strategy to mitigate the aerodynamic responses under a broad range of design wind speeds. This study investigates the possibility of producing similar behavior of side protrusion via a corner protrusion strategy. The proposed strategy is evaluated using two parameters, which are the gap ratio (GR) and the protrusion ratio (PR). High-frequency force balance (HFFB) wind tunnel testing was carried out to examine the aerodynamic performance of ten models under different wind angles. The results demonstrate that the corner protrusion strategy can achieve similar performance as the side protrusion strategy using nonstructural components (NCs). The reductions of base overturning moment (OTM) for model CP-14–86 are 33%, 39%, 33%, and 24% at the mean hourly design wind speeds (cities) of 42 m/s (San Francisco), 53 m/s (New York), 62 m/s (Houston), and 77 m/s (Miami), respectively. The effectiveness of the corner protrusion strategy occurs when the PR is larger than 6%. The benefits of using NCs to reduce wind responses of tall buildings are discussed, which is expected to be a competitive aerodynamic strategy not only for new buildings but also for retrofitting existing buildings.

1. Introduction

For high-rise buildings, the mitigation of aerodynamic responses over a broad range of wind speeds is important when it comes to various design objectives, such as habitability, serviceability, and survivability design [1]. The effectiveness of external shape modification, which is referred as aerodynamic strategy in this study, on the wind behavior of high-rise buildings is well documented in some recent review papers [19,35,39]. The aerodynamic shape of the building affects the position of flow separation (and reattachment, if any) and similarly the vortex shedding frequency. An appropriate aerodynamic strategy can reduce wind design demands, leading to the desired design objectives with lower construction and maintenance cost.

The aerodynamic strategy of high-rise buildings can be roughly divided into: (1) height modification, such as tapering [6,25], setback [21,44], or twisting [26]; and (2) cross-section modification, which is the focus of this study. Currently, most of existing studies of cross-section modification concentrate on corner modification strategy, including chamfered [9,10,20,22,24,42–44,46], recessed [9,44,46], and rounded [2,20,43]. In addition to academic research, this strategy has also been successfully applied to one of the world's tallest skyscrapers, Taipei 101, resulting in a reduction of 25% in base moment demands [18]. Although the benefits of the corner modification strategies are well recognized in the community of wind engineering, the original floor area is normally reduced and converted to an irregular shape due to the constraint of footprint, which might not be preferred from the perspective of owners.

Building on the work in traditional corner modification strategies, Lu et al. [32] conducted a systemic study of cross-section modifications, including (1) subtractive (e.g., corner recession), (2) additive (e.g., side protrusion), and (3) the hybrid of both strategies (see Fig. 1) from the perspective of a square benchmark model. The models presented in Fig. 1 are designated by "corner type"-"side type". For corner type, B and S represent basic corner and single corner recession corner, respectively. There are three side types, which are: basic side (B), U-shape side protrusion (U), and wide side protrusion (W). Other than the subtractive strategy (Fig. 1(b)), the floor area can be maintained or increased using the additive (Fig. 1(c)) or the hybrid (Fig. 1(d)) strategies while achieving better aerodynamic performance of high-rise buildings over a broad range of design wind speeds. The base overturning moment (OTM) for the models with subtractive (S-B) and additive strategies (B-W and B-U) normalized by the benchmark model is presented in

* Corresponding author.
E-mail address: brian.phillips@essie.ufl.edu (B.M. Phillips).

https://doi.org/10.1016/j.engstruct.2024.118055
Received 25 July 2023; Received in revised form 1 April 2024; Accepted 12 April 2024
Available online 26 April 2024

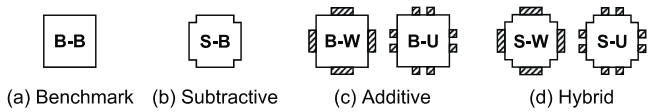

Fig. 1. Plan view of various cross-section aerodynamic strategies [32].

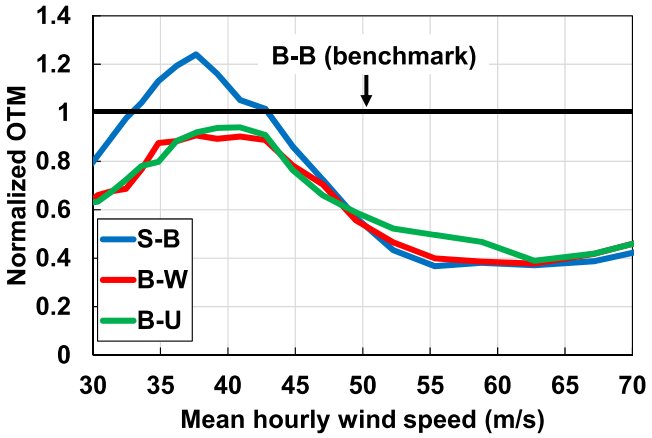

Fig. 2. Normalized OTM of subtractive and additive cross-section aerodyanmic strategies at various design wind speeds [32].

Fig. 2.

The responses of the hybrid strategy are not included since it is not the focus of this study. In Fig. 2, the results show the effectiveness of the subtractive strategy in reducing the OTM under high-wind speeds. For example, the OTM of S-B is reduced by more than 40% for wind speeds higher than 50 m/s. However, the responses for S-B over low wind speeds (e.g., 35 m/s to 40 m/s) are amplified up to 20%. This amplification attributed to the increase of vortex shedding frequency, which is another downside of the subtractive strategy [32]. Conversely, the potential of additive strategies by adopting side protrusion can be observed based on the reduction of OTM for B-W and B-U throughout the wind speeds of 30 m/s to 70 m/s, which provides a different option for designers and owners if the footprint can be increased.

As shown in Figs. 1 and 2, the similar performance between B-W and B-U implies that the middle portion of the B-W side protrusion is not significant to the overall behavior. This represents that the same wind design demands can be achieved using various external shapes for a tall building. However, it is not clear if the aerodynamic performance of B-U will be influenced by further increasing the gap in the side protrusion, which is the first objective of this study. If the desired behavior can be maintained with a larger gap in the protrusion, this can provide more flexibility for design objectives beyond aerodynamic responses, such as floor area, operation purposes, and aesthetics. Furthermore, the protrusion strategy might be able to be achieved via nonstructural components (NCs) instead of changing the external shape if the gap is large enough. Since the influence of NCs on the mass, damping, and stiffness for a building is expected to be limited, this could be a more efficient design process if there are multiple strategies to compare.

In the past decade, the potential of applying NCs on the surface of tall buildings has gained growing attention to achieve various objectives, including energy saving [38], energy harvesting [11], ventilation [34,50], solar shading [48], and aerodynamic behavior. Table 1 provides an overview of studies on the aerodynamic behavior of buildings with various NCs using computational fluid dynamics and physical wind tunnel testing. The information presented in the table includes research approach, aerodynamic strategy, protrusion ratio, wind direction, building height, and performance indicator.

As listed in the table, the nonstructural components can be façades (also called ribs or plates in different studies) [5,7,15,17,27–31,49,52], mullions [41], double-skin façades [12–14,40], and curtain walls [37]. The protrusion ratios of NCs vary from 1.6% to 16% relative to the width of the building. Based on the orientation of the NCs, the aerodynamic strategies can be roughly divided into (1) vertical orientation, (2) horizontal orientation, and (3) the hybrid of both. In the literature, the NCs have significant influence on the flow characteristics, local pressure coefficients, and aerodynamic coefficients of high-rise buildings. For flow characteristics, Liu et al. [30] reported that the size of wake vortex

Table 1
Overview of studies on the aerodynamic behavior of buildings with various NCs.

Reference	Research approach	Aerodynamic strategy	Protrusion ratio	Wind direction (°)	Building height	Performance indicator
Stathopoulos and Zhu [41]	SMPM	Mullion (vertical)	1.6 % and 3.2 %	0° – 180°	15 m and 120 m	PC
Quan et al. [37]	SMPM and HFFB	Curtain wall	3.6 %	0° – 360°	206 m	PC, AC, PSD
Hu et al. [13]	SMPM and Aero	DSF (vertical)	5 %	0°	180 m	PC, PSD SR
Yuan et al. [52]	SMPM	Plate (horizontal)	7.5 %, 10 %, and 12.5 %	0° – 45°	150 m	PC
Hui et al. [17]	SMPM	Plate (horizontal)	7.5 %, 10 %, and 12.5 %	0° – 45°	150 m	PC, AC, PSD
Hu et al. [14]	SMPM and PIV	DSF (vertical)	5 %	0°	180 m	PC, PSD, FF
Yang et al. [49]	SMPM	Plate (vertical)	7.5 % and 12.5 %	0° – 90°	150 m	PC, AC, PSD
Cheng et al. [7]	SMPM and HFFB	Façade (horizontal, vertical, and hybrid)	2 % and 4 %	0° – 360°	200 m	PC, AC
Liu et al. [29]	SMPM and PIV	Rib (horizontal and vertical)	12.5 %	0°	150 m	PC, AF, FF
Liu et al. [28]	CFD	Rib (vertical)	2 %– 16 %	0°	-	PC, AC, and FF
Chen et al. [5]	SMPM	Façade (horizontal, vertical, and hybrid)	1.6 %	0° – 90°	183 m	PC
Hui et al. [15]	CFD	Rib (vertical)	10 %	0°	-	PC, AC and FF
Liu et al. [27]	CFD	Rib (vertical)	0 %– 14 %	0° and 45°	-	PC, AC and FF
Hou et al. [12]	AERO	Smart morphing DSF	4.8 %	0° – 90°	184 m	SR
Skvorc and Hozmar [40]	SMPM and HFFB	Porous DSF	5 %	0° – 45°	200 m	PC, AC, PSD
Liu et al. [30]	CFD	Rib (horizontal, vertical, and hybrid)	6 %	0°	80 m	PC, FF
Liu et al. [31]	CFD	Rib (horizontal)	6 %	0°	80 m	PC, FF

Protrusion ratio is defined as the depth of the protrusion divided by the width of the building. SMPM: simultaneous multi-channel pressure measurement, HFFB: high-frequency force balance, PIV: particle image velocimetry, AERO: aeroelastic testing, PC: pressure coefficient, AC: aerodynamic coefficient, PSD: power spectral density, SR: structural response, DSF: double-skin façade, CFD: computational fluids dynamics FF: flow field

is influenced by the horizontal facades, and the flow separation and shear layer are affected by vertical facades. The change of local pressure coefficients is significantly influenced by the positions of façades [7]. The reduction of the local pressure coefficients can be reduced by more than 20% with various protrusion ratios [5,37,52]. For aerodynamic coefficients, it was demonstrated that vertical facade is a more effective strategy than that of horizontal facade [17,27,30]. Regarding the effectiveness, the standard deviation (or fluctuating) of lift coefficients can be reduced by more than 50% with protrusion ratios vary from 6% to 12.5% [15,27,28,30,31,49].

As discussed in the literature review, it is well-known that the impact of NCs on the local pressure coefficients is significant, which can benefit to the design of components and cladding (C&C). For main wind force resisting system (MWFRS) design, however, the reduction of design demands under various wind speeds received much less attention in the literature, which is a topic that should not be ignored. Since the structural responses (e.g., OTM, roof drift, and acceleration) of tall buildings under wind loading are velocity/frequency dependent [1,23,45,53], it is not clear how large the influence of NCs can have for different cities with different design wind speeds solely based on the reductions of aerodynamic coefficients. Moreover, shifts toward performance-based wind engineering will require the consideration of structural responses at multiple wind speeds spanning habitability, serviceability, and survivability. Therefore, the second objective of this study is to examine the influence of various protrusion ratios targeting at using NCs on the aerodynamic performance of tall buildings at different wind speeds, as indicated by the full-scale structural response.

To summarize, the two objectives are (1) to investigate the potential of corner protrusion strategy using nonstructural components for MWFRS design, and (2) to identify effective corner protrusion ratios. A total of ten models, including a square benchmark model, are generated in this study. A well-recognized cross-section modification strategy is taken as a starting point to investigate the influence of gap size in the protrusion (for the first objective) and the protrusion depth (for the second objective) for a corner protrusion strategy. High-frequency force balance (HFFB) testing was conducted to capture the aerodynamic behavior of each model under various wind angles. The peak OTM was used to evaluate the full-scale structural responses at a broad range of wind speeds considering the time (mean and background components) and frequency domain (resonant component) results.

This paper is organized as follows: model description is presented in Section 2, followed by the experimental method and evaluation approach in Section 3. The aerodynamic performance for each model is discussed in Section 4. The conclusions are summarized in Section 5.

2. Model description

The plan views of the ten models considered in this study are presented in Fig. 3. The models are all doubly-symmetric in cross-section and prismatic along the height. The 40 cm tall models represent a 300 m tall building at 1:750 scale with various plan dimensions. SQ70 (the model with a square 70 mm × 70 mm cross-section) is taken as the benchmark to compare with the other aerodynamic modification models, which are all considered as additive strategies because of a larger footprint in comparison with the benchmark model. The aerodynamic modification models are designated by CP-PR-GR. CP denotes Corner Protrusion. The PR (protrusion ratio) and GR (gap ratio) are the two parameters for the corner protrusion strategy. PR indicates the ratio between the protrusion length and nominal building width (70 mm), and GR indicates the ratio between the width of the gap in the side protrusion and the nominal building width (70 mm). For example, CP-14–43 has 10 mm-protrusion length (10 mm / 70 mm = 14%) and 30 mm-gap in the protrusion (30 mm / 70 mm = 43%). As found in the literature, a PR of 0% to 14% is selected as it is a reasonable range for NCs to achieve. GR was selected to vary from 0% to 86%. The combination of PR and GR creates the models shown in Fig. 3; the grey areas indicate what make each model unique while the white area is the underlying benchmark model dimensions.

CP-14–0 is taken as the initial side protrusion strategy to study the influence of GR and PR on the wind performance of tall buildings. It is worth mentioning that CP-14–0 is also a well-recognized corner recession strategy from the perspective of subtractive design with an 11% modification ratio from a baseline 90 mm × 90 mm plan model. However, it is not clear if CP-14–0 will perform better than SQ70 under various wind speeds, which is the preliminary task that needs to be confirmed before discussing the two objectives.

For the first objective, the GR is varied to investigate feasibility of using the corner protrusion strategy to imitate the behavior of CP-14–0. The gap sizes for CP-14–0, CP-14–14, CP-14–43, CP-14–71, and CP-14–86 are 0 cm, 1 cm, 3 cm, 5 cm, and 6 cm, respectively. CP-14–86 (the model with the largest GR) is regarded as the corner protrusion strategy achieved via NCs. The narrowest protrusion is 5 mm wide, selected to avoid local vibrations under wind tunnel testing using the foam material. Next, the protrusion lengths are decreased from 10 mm (CP-14–86) to 2 mm (CP-3–86) with a 2 mm decrement, all with a fixed GR of 86%. The purpose of this is to examine the effects of the protrusion length on the corner protrusion strategy using NCs. All models are prismatic throughout the height, representing that the corner protrusion strategy is in vertical orientation. The photographs of SQ70, CP-11–86, and CP-6–86 are presented in Fig. 4.

3. Experimental method and evaluation approach

3.1. HFFB testing setup

HFFB wind tunnel testing [45] was carried out in the boundary layer wind tunnel (BLWT) at the University of Florida (UF) (see Fig. 4). The UF BLWT is an open-circuit wind tunnel that measures 3 m high × 6 m wide × 38 m long. A length scale of 1:750 was selected to generate a suburban terrain condition with power-law index of 0.22 using the Terraformer [3,4]. The configuration of the Terraformer was set to a uniform height of 31 mm at 0° (wide) orientation. A terrain extension sheet was

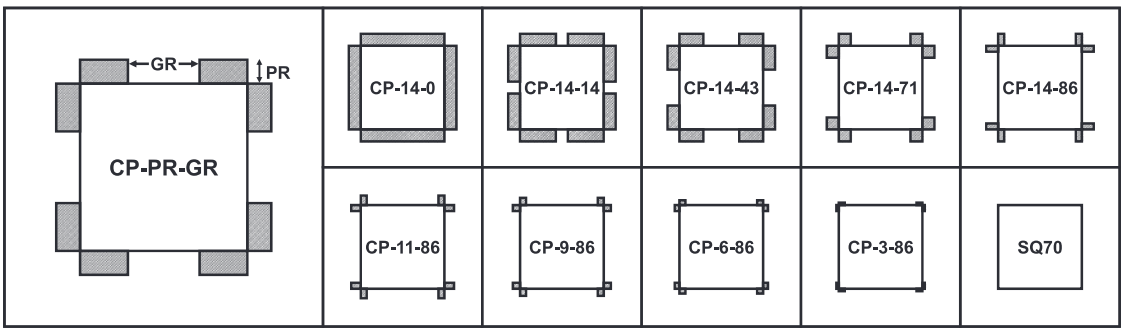

Fig. 3. Plan view of ten models.

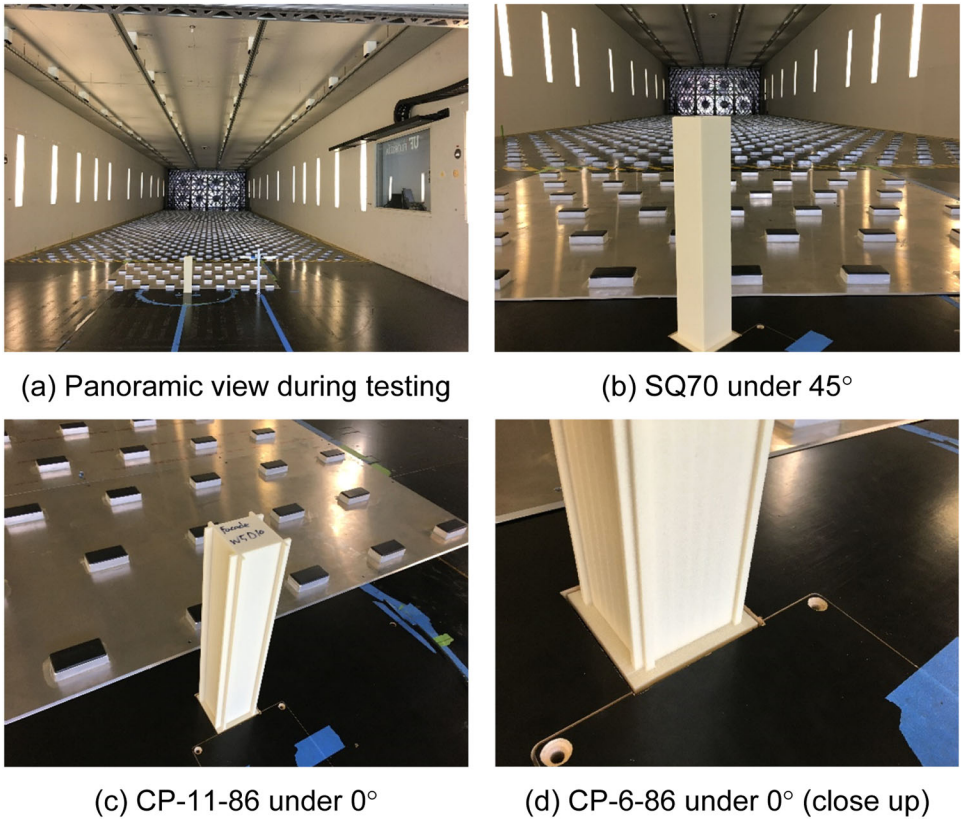

Fig. 4. Photographs of HFFB testing in the UF BLWT.

installed in the downwind of the Terraformer to maintain the desired approach flow condition over the turntable. Fig. 5(a) and (b) show the mean wind speed and turbulence intensity in the longitudinal direction at the center of the test section. The mean wind speed at model height was 9.8 m/s, corresponding to a Reynolds number of 4.5×10^4 based on the width of the benchmark model. The power spectral density (PSD) of the approach flow in the longitudinal direction at the top of the model is plotted in Fig. 5(c).

The external shapes of the ten models were produced from a light-weight high-density foam material. Inside the model, a 25.4 mm outer diameter hollow aluminum rod with 3.175 mm wall thickness was used to provide sufficient stiffness for the force-balance system. During HFFB testing, a TFI cobra probe was placed 40 cm above the ground (model height) offset in the across-wind direction to measure the reference wind velocity. Because all models are doubly-symmetric in cross-section (see Fig. 3), a span of 45° is sufficient to capture responses from 0° to 360°. A total of 10 wind angles from 0° to 45° at 5-degree increments for each model were tested. A six-axis load cell (ATI Industrial Automation, Delta model) was used to capture the base responses. Time series data were recorded at 2000 Hz for 1 min for each wind angle using a dSPACE MicroLabBox real-time processor.

3.2. Post-processing procedure

The flowchart of HFFB post-processing procedure is presented in Fig. 6(a). For each wind angle, the time series data of base moments in the along-wind and the across-wind directions were used to evaluate the aerodynamic performance. Along-wind and across-wind are the response axes, referred to the global coordinate system of the wind tunnel (relative to the wind direction). The data were filtered through a low-pass Butterworth filter with a cutoff frequency of 30 Hz to remove the physical model resonance in the time domain and frequency domain results. The mean, background, and resonant components are used to generate structural responses for each model. As mentioned in the

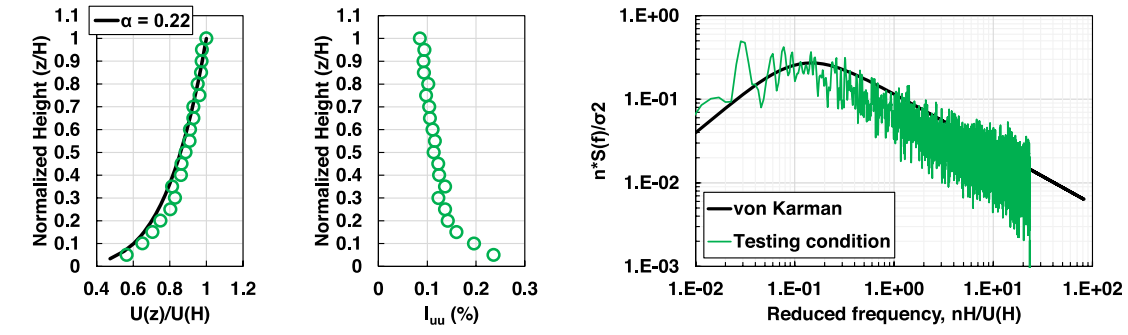

Fig. 5. Approach flow conditions of wind tunnel testing (H = 40 cm, U(H) = 9.8 m/s).

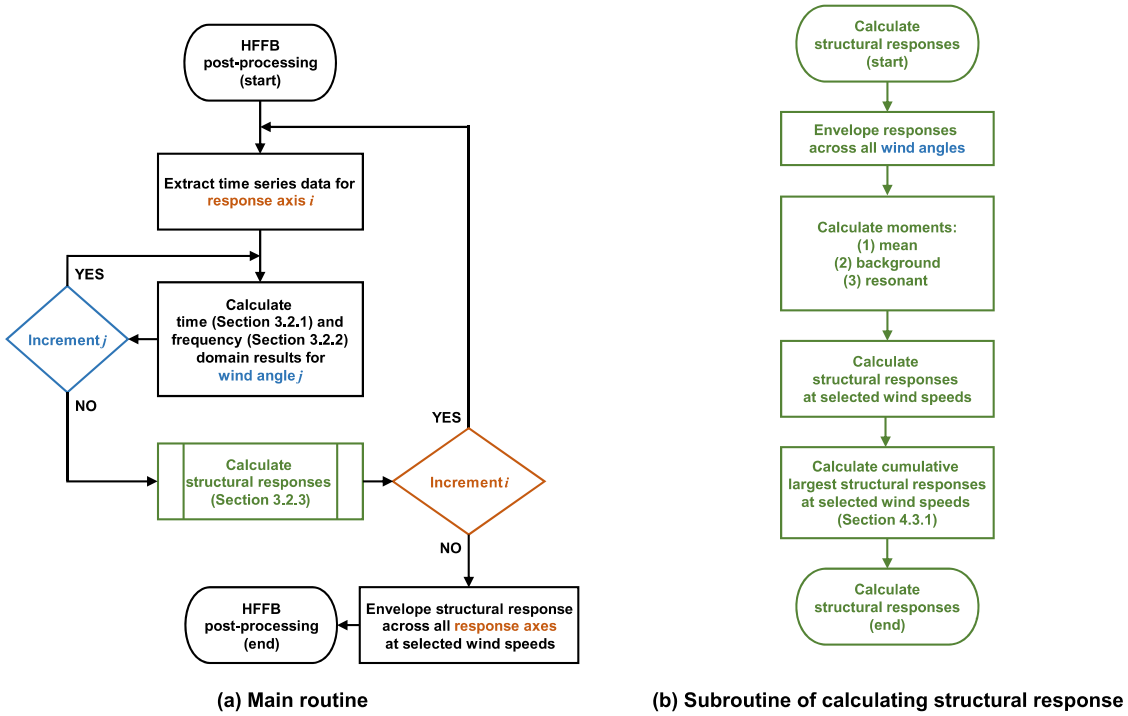

Fig. 6. Flowchart of HFFB post-processing procedure.

introduction, the structural responses of a building can be OTM, roof drift, and acceleration. To avoid any confusion, in this study, "structural response" refers to the OTM. Torsional responses, another response axis, were below the manufacturer's stated resolution of the load cell and were not included in analysis. The analysis process is discussed below.

3.2.1. Base moment coefficients in time domain

In the time domain, the mean and standard deviation (STD) statistics in both along-wind and across-wind are calculated from the time series data for each wind angle. The statistics are normalized by $\frac{1}{2}\rho U^2 BH^2$ where ρ is the air density, U is the mean wind speed at model height (9.8 m/s), B is the model width (0.07 m), and H is the model height (0.4 m). The four non-dimensional base moment coefficients are $\overline{CMD}$ (mean component in along-wind), $\overline{CML}$ (mean component in across-wind), σ_{CMD} (background component in along-wind), and σ_{CML} (background component in across-wind).

3.2.2. PSD responses in frequency domain

In the frequency domain, the PSD responses ($f * S(f)$) with respect to the reduced frequency are calculated for each wind angle in both along-wind and across-wind directions. The reduced frequency (f_R) can be expressed as:

$$f_R = \frac{f * B}{U} = \frac{f_1 * B_F}{U_F} \tag{1}$$

where f is the model-scale excitation frequency. The corresponding full-scale wind speeds (U_F) at building top can be determined based on Eq. (1). The full-scale fundamental frequency (f_1) is assumed to be 0.1 Hz. Based on the length scale of 1:750, the full-scale building width (B_F) and height (H_F) are 52.5 m and 300 m, respectively. With the cutoff frequency of 30 Hz, the upper bound of f_R that can be investigated is 0.21 (30 Hz × 0.07 m / 9.8 m/s), corresponding to a lower bound full-scale wind speed of 25 m/s (0.1 Hz × 52.5 m / 0.21). The highest full-scale wind speed of interest at the building top is 85 m/s, corresponding to a f_R of 0.06 (0.1 Hz × 52.5 m / 85 m/s).

3.2.3. Full-scale structural responses

Based on the assumption of a Gaussian process, the full-scale peak base over-turning moment (OTM) can be expressed as [23,53]:

$$\widehat{M}(f) = \overline{M} + \sqrt{M_B^2 + M_R^2(f)} \tag{2}$$

where $\widehat{M}(f)$ is the full-scale peak OTM, $\overline{M}$ is the full-scale mean OTM, M_B is the full-scale background dynamic OTM, and M_R is the full-scale resonant OTM. Eq. (2) is calculated independently for the along-wind and across-wind directions.

In Eq. (2), responses vary with wind angle. Since the largest responses do not always occur at the wind angle of 0° when aerodynamic strategies are applied [32], the envelope or dominant responses across all wind angles is extracted for each component independently (along versus across wind) to avoid an unconservative design.

The full-scale mean ($\overline{M}$) and STD (σ_M) OTMs can be determined based on the moment coefficients ($\overline{CMD}$ and σ_{CMD} for along wind and $\overline{CML}$ and σ_{CML} for across wind) obtained from the time domain results multiplied by $\frac{1}{2}\rho U_F^2 B_F H_F^2$. The full-scale background OTM can be expressed as:

$$M_B = g_B * \sigma_M \tag{3}$$

where g_B is the gust factor for the background component. The full-scale resonant component can be expressed as:

$$M_R(f) = g_R * \sigma_M * \sqrt{\frac{\pi}{4} * A(f) * \frac{1}{\zeta}} \tag{4}$$

where g_R is the gust factor for the resonant component, ξ is the full-scale building damping ratio, and $A(f)$ is the amplification factor for the resonant component, which can be expressed as:

$$A(f) = \frac{f * S(f)}{\sigma^2_{M\_HFFB}} \tag{5}$$

where σ_{M_HFFB} is the model-scale STD moment response obtained from wind tunnel testing. The gust factors for the background and resonant

components are assumed to be 3.5 [23,45,53]. A 1% damping ratio is assumed for the models considered under all wind speeds.

Because the resonant component does not change linearly with wind speed/reduced frequency, the cumulative largest responses for MWFRS design at different wind speeds is considered to avoid an unconservative design, which will be discussed along the structural response in Section 4.3.1. Additionally, it is needed to identify the dominant axis of the structural response of interest, which is normally controlled by the frequency domain results in the across-wind direction (will be discussed in Section 4.2.1).

4. Results of wind tunnel testing

This section compares the aerodynamic performance of the ten models under wind loading. The time domain results (base moment coefficients) are presented in Section 4.1. The frequency domain results (PSD responses) are discussed in Section 4.2. The full-scale OTM for the MWFRS under various wind speeds considering all wind angles are examined in Section 4.3. A brief discussion is presented in Section 4.4.

4.1. Time domain results

4.1.1. Largest base moment coefficients across all wind angles

Fig. 7 shows the largest values of mean and STD base moment coefficients enveloped over all wind angles for the ten models in along-wind and across-wind directions. For mean moment coefficients (Fig. 7(a)), the responses are dominated by the along-wind direction for all models. The $\overline{CMD}$ for the benchmark model (SQ70) and CP-14–0 are 0.66 and 0.75, respectively. The larger response of CP-14–0 indicates that increasing the footprint of a building (additive aerodynamic strategy) do not benefit to $\overline{CMD}$. With respect to the effects of PR, it can be observed that the $\overline{CMD}$ is increased through SQ70 to CP-14–86. The largest $\overline{CMD}$ is 0.92 occurs at CP-14–86, which is 39% larger than that of SQ70. Because of negligible resonant component in the along-wind direction (will be discussed in Section 4.2), the amplification of $\overline{CMD}$ due to corner protrusion is not expected to increase the design demand for the MWFRS of tall buildings. However, more attention is needed when it comes to C&C design, such as curtain walls or windows.

Regarding the STD moment coefficients (Fig. 7(b)), the responses are not solely dominated by along or across wind. For example, the STD moment coefficients for CP-14–71, CP-14–86 and CP-11–86 are dominated by the along-wind direction (σ_{CMD}), and CP-6–86, CP-3–86 and SQ70 are dominated by the across-wind direction (σ_{CML}). For the benchmark model, the across-wind STD moment coefficient (σ_{CML}) is 0.166. Regarding the effectiveness of increasing footprint of a building (additive aerodynamic strategy), the σ_{CML} of CP-14–0 is decreased to 0.133, equivalent to 20% reduction in comparison with the benchmark model.

With respect to GR, the effectiveness in reducing σ_{CML} is preserved for various GRs, showing that the aerodynamic performance is not sensitive to the gap in the side protrusions for the background component. In general, the structural responses of high-rise buildings are dominated by the dynamic responses in the across-wind direction [8,32]. Although the σ_{CMD} responses are increased with larger GRs (see Fig. 7(b)), the possibility of using the corner protrusion strategy to achieve the same ideal aerodynamic performance in across-wind as CP-14–0 is demonstrated.

With respect to the effects of PR, the σ_{CML} responses for CP-3–86 (3% PR) and CP-6–86 (6% PR) are 0.166 and 0.165, respectively (see Fig. 7 (b)). In comparison with the benchmark model, there is no reduction of σ_{CML} for the two models. For models with a larger PR, the σ_{CML} responses for CP-9–86 (9% PR) and CP-11–86 (11% PR) are 0.142 and 0.129, respectively, which are equivalent to 14% and 22% reduction. The results indicate that a PR larger than 6% is needed to suppress the across-wind background component (derived from σ_{CML} as in Eq. 3) for models with the corner protrusion strategy.

4.1.2. Base moment coefficients at various wind angles

The envelope over all wind angles was the focus of the previous section. This section investigates the influence of GR on base moment coefficients for each model under various wind angles, plotted in Fig. 8. In along-wind (Fig. 8(a) and (b)), although the responses for aerodynamic modification models are decreased for wind angles of 0° to 10°, both the $\overline{CMD}$ and σ_{CMD} are increased when the wind angles are larger than 15° in comparison with the benchmark model. This situation is more significant for CP-14–86, whose largest values, occurred at 45°, are clearly larger than that of the benchmark model. For example, the largest $\overline{CMD}$ for CP-14–86 is 39% larger than that of SQ70 (discussed in Section 4.1.1). The results indicate that the side protrusion and the corner protrusion strategy cannot reduce the aerodynamic coefficients in the along-wind direction when all wind angles are considered.

For $\overline{CML}$ (Fig. 8(c)), the responses are significantly suppressed under wind angles of 10° to 20°, which are the critical wind angles for the benchmark model. For σ_{CML}(Fig. 8(d)), although the responses are increased for wind angles larger than 15°, the peak values across all wind angles for the aerodynamic modification models are still smaller than that of the benchmark model.

Regarding the influence of GR, the results seem to suggest that the aerodynamic coefficients are not sensitive to the gap in the middle of side protrusion for the models with GR smaller than 71%. From CP-14–71 to CP-14–86, the increase of responses for wind angles of 25° to 45° (see Fig. 8(a), (b), and (d)) indicate the flow characteristics for the

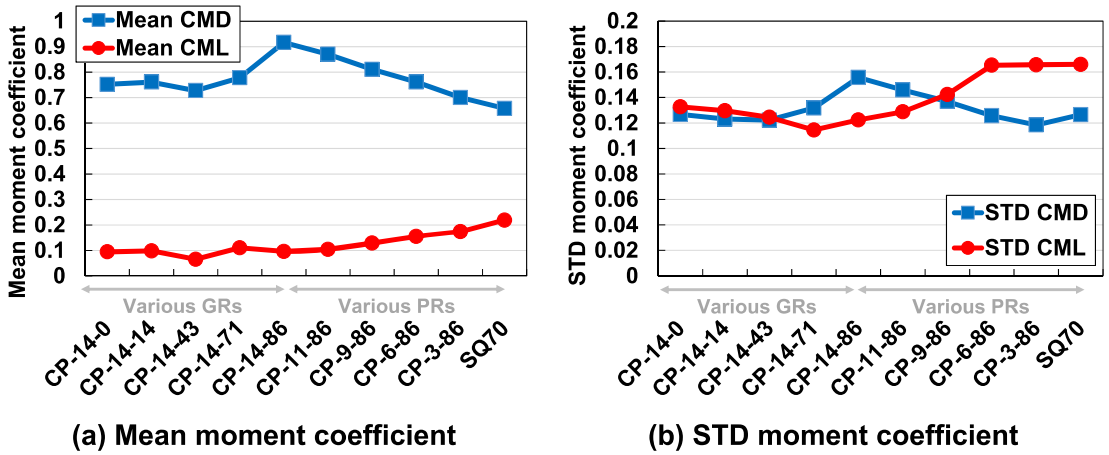

Fig. 7. The largest base moment coefficients across all wind angles.

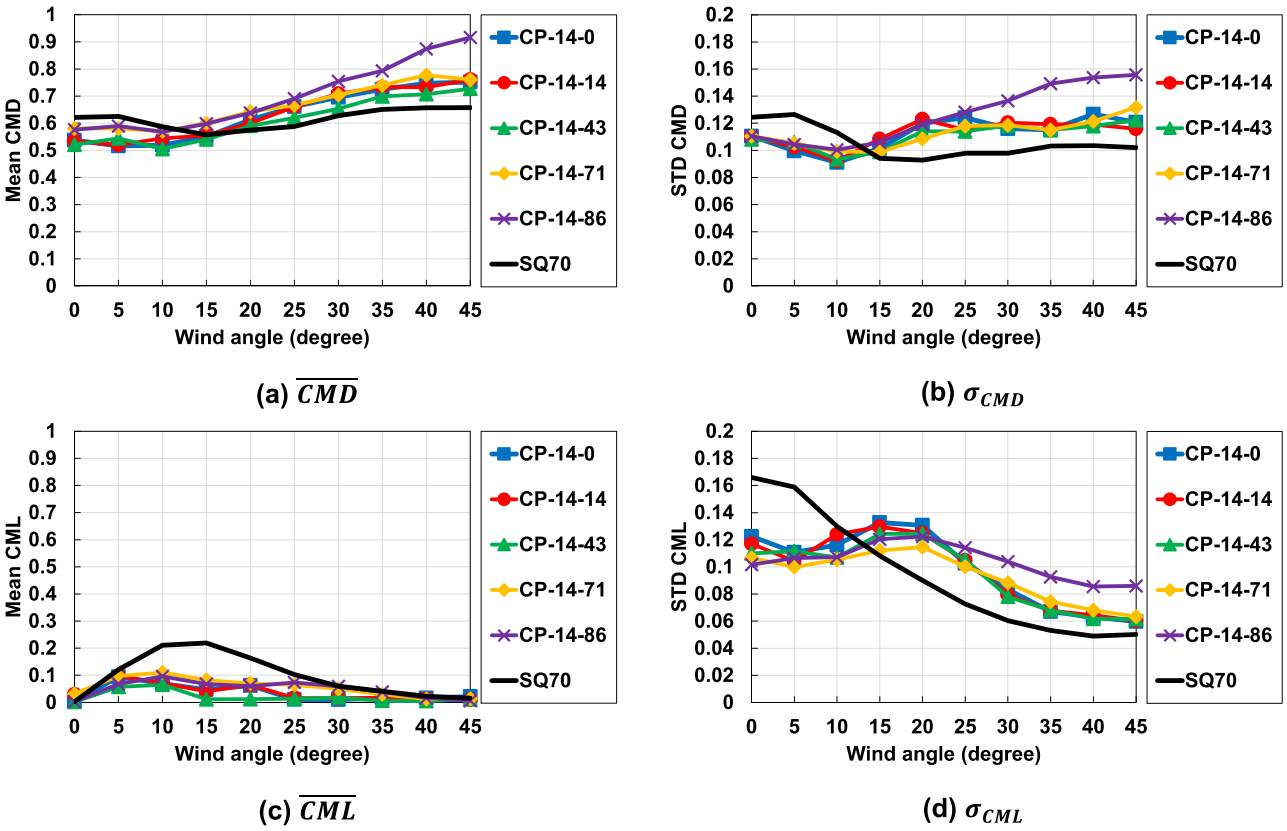

Fig. 8. Base moment coefficients for models with various gap ratios (GRs).

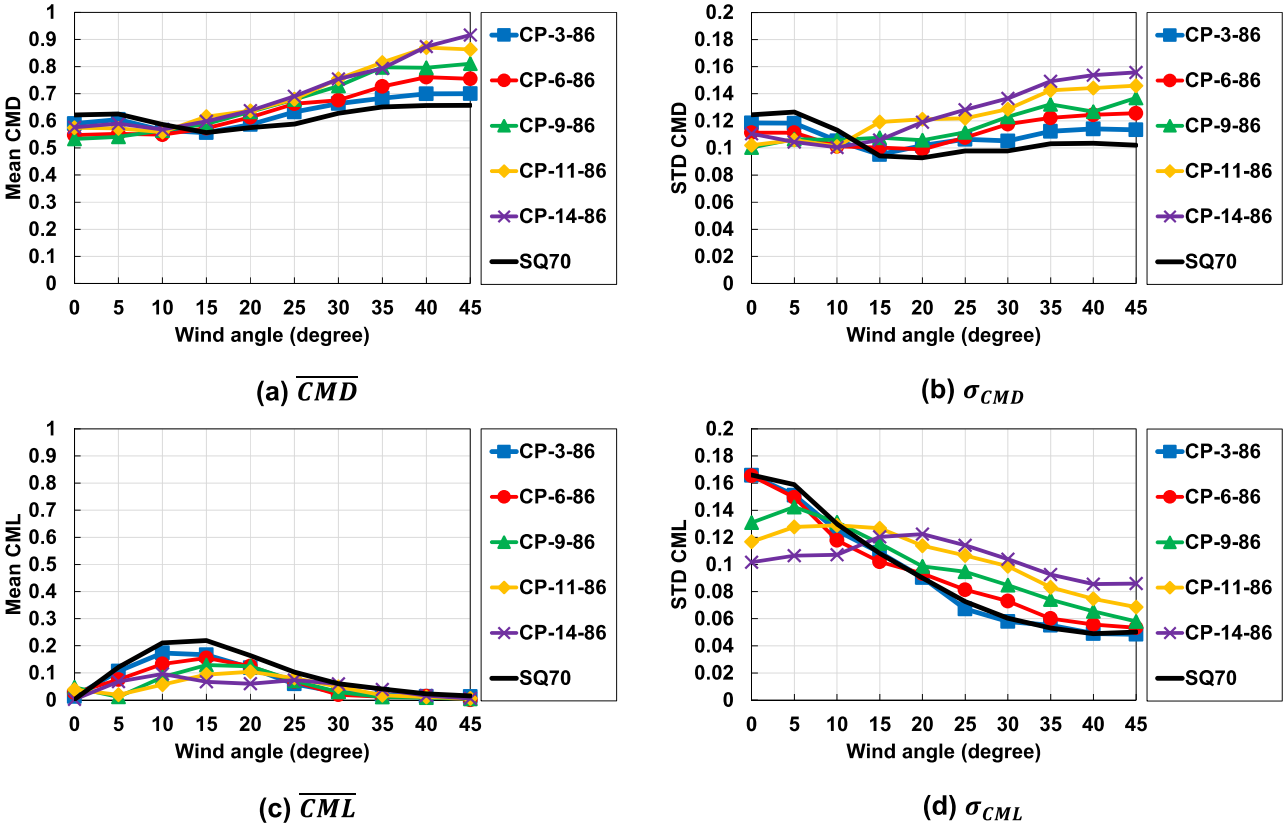

Fig. 9. Base moment coefficients for models with various protrusion ratios (PRs).

corner protrusion strategy (CP-14–86, 5 mm width for the protrusions) are different for the model with larger protrusion width (larger than 10 mm) at the wind angles. The mechanism behind this needs flow visualization techniques, such as CFD or PIV, to confirm. Even so, it is worth emphasizing that CP-14–86 is still a competitive strategy to suppress the mean and background components when it comes to the MWFRS design.

The influence of PR on aerodynamic coefficients under different wind angles is presented in Fig. 9. As shown in Fig. 9(a) and (b), the adverse effects of corner protrusion strategy in along-wind for models with larger PRs (discussed in Fig. 7) is attributed to the increase of responses for wind angles of 20° to 45°. The strategy does not lead to any unfavorable effect for $\overline{CML}$ (see Fig. 9(c)). For σ_{CML} (Fig. 9(d)), the responses of CP-3–86 and CP-6–86 are almost identical to the benchmark model, confirming that a PR smaller than 6% for the corner protrusion strategy does not benefit the background components under any wind angles. For models with a PR larger than 6% (CP-9–86, CP-11–86, and CP-14–86), although the responses are increased at wind angles larger than 20°, the peak values of σ_{CML} are still smaller than that of the benchmark model, which can reduce the design demands of MWFRS for tall buildings.

This section discussed the time domain results of the ten models under wind angles of 0° to 45°. Among the mean and background components in along-wind and across-wind directions, the $\overline{CMD}$ produces the largest magnitudes and σ_{CML} is a critical response for the design of MWFRS. For $\overline{CMD}$ and σ_{CML}, the responses of wind angles of 0° to 10° for aerodynamic modification models are smaller, while the responses of wind angles larger than 15° are larger than that of the benchmark model. This indicates the need to consider all possible wind angles to achieve a conservative design for tall buildings. Regarding enveloping responses, the largest $\overline{CMD}$ responses for aerodynamic modification models are larger than that of the benchmark model, suggesting a potential drawback for C&C design. For σ_{CML}, although the responses are increased for some wind angles, the envelope responses for aerodynamic modification models are all smaller than that of the benchmark model. Regarding MWFRS design, the effectiveness of the protrusion strategy is increased with PR and not sensitive to GR.

4.2. Frequency domain results

4.2.1. The envelope of PSD responses across all wind angles

Fig. 10 shows the envelope of PSD responses across all wind angles for the models with various GRs. As discussed in Section 3, the upper bound and lower bound of interested reduced frequencies (design wind speeds) are 0.21 (25 m/s) and 0.06 (85 m/s), respectively. In Fig. 10, the PSD responses in along-wind are significantly smaller than that of across-wind over the range of the frequencies of interest. Because of the gust and amplification factors in Eq. 4, the structural responses are expected to be dominated by the across-wind direction. In other words, the impact of the observations in Section 4.2 are much more significant than those in Section 4.1. Therefore, the design of MWFRS for the aerodynamic modification models should not be influenced by the worse base moment coefficients obtained in the along-wind direction.

In Fig. 10(b), the dominant reduced frequency (or Strouhal number) for SQ70 is 0.1. It can be observed that the PSD responses for CP-14–0 are smaller than that of SQ70 throughout the reduced frequencies considered, suggesting the effectiveness to mitigate resonant responses under various wind speeds using the side protrusion strategy. The reasons are attributed to (1) the peak PSD responses are significantly reduced, and (2) the dominant reduced frequency is maintained the same as the benchmark model, which is a feature that cannot be achieved using subtractive aerodynamic strategy. I.e., a corner recession cut into SQ70 would lead to adverse responses (as compared to SQ70) at lower wind speeds [32].

With respect to the influence of GR, the similar PSD responses between various models across different reduced frequencies (see Fig. 10 (b)) indicates that the resonant responses are not influenced much by the gap in the side protrusion strategy. This shows the feasibility of using the corner protrusion strategy to achieve similar performance as the side protrusion strategy (CP-14–0).

The envelopes of PSD responses for the models with various PRs in along-wind and across-wind directions are shown in Fig. 11(a) and (b), respectively. The same as Fig. 10, the resonant responses are dominated by the across-wind direction. In Fig. 11(b), the reduction of peak PSD is more significant for models with a larger PR. This behavior is also observed from the whole range of the reduced frequencies. The PSD responses for CP-3–86 and CP-6–86 are only reduced by a narrow range of reduced frequencies in comparison with CP-14–86. This indicates that a PR smaller than 6% can only provide limited reduction in the resonant component over a small range of design wind speeds. For CP-9–86, CP-11–86, and CP-14–86, the results show that the corner protrusion strategy is an effective strategy to alleviate the dynamic responses for tall buildings over a broad range of design wind speeds.

4.2.2. Across-wind PSD responses at different wind angles

To further dive in the effect of the approaching wind angles, the across-wind PSD responses under various wind angles for the models with different PRs are shown in Fig. 12. For the benchmark model (Fig. 12(a)), the resonant responses are dominated by the wind angles of 0° and 5° throughout different reduced frequencies. When wind angles are larger than 15°, the dynamic responses are negligible. The trends of critical wind angles remain the same for CP-3–86 (Fig. 12. (b)) and CP-6–86 (Fig. 12. (c)). The patterns for dominant wind angles for the corner protrusion strategy change in between the PR of 6% and 9%. For CP-9–86 (Fig. 12(d)), the dominant wind angle occurs at 5°. As PR further increased, the peak responses are controlled by 10° and 15° for CP-11–86 and CP-14–86, respectively.

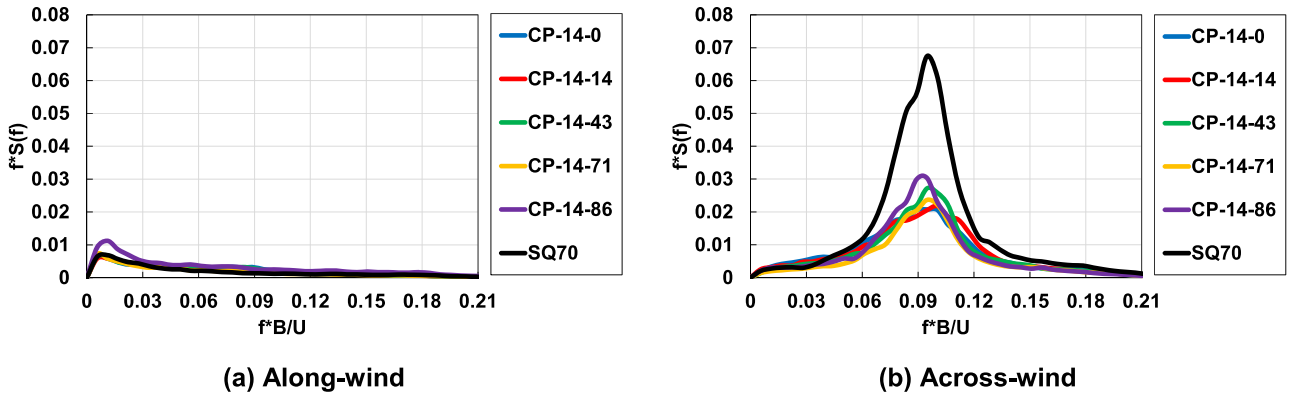

Fig. 10. Envelope of PSD responses for models with various gap ratios (GRs).

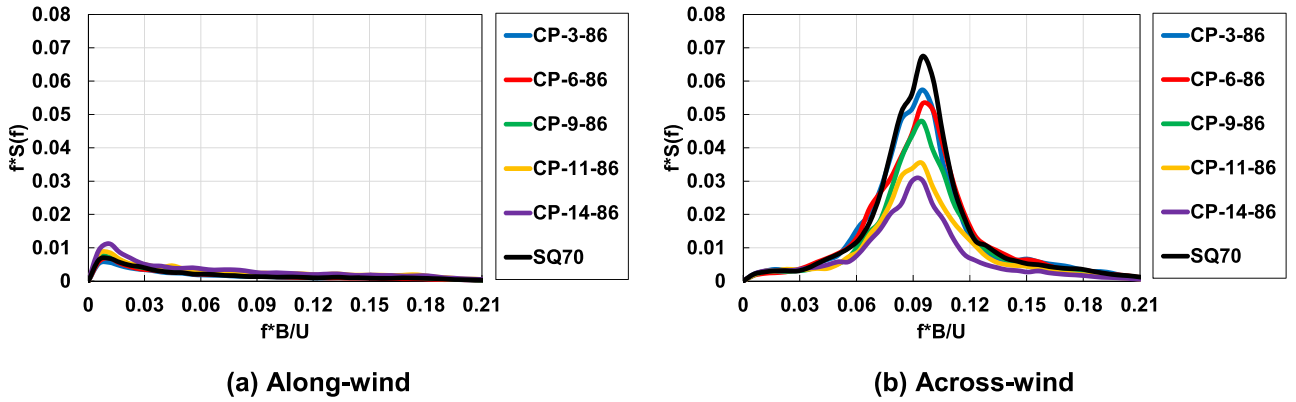

Fig. 11. Envelope of PSD responses for models with various protrusion ratios (PRs).

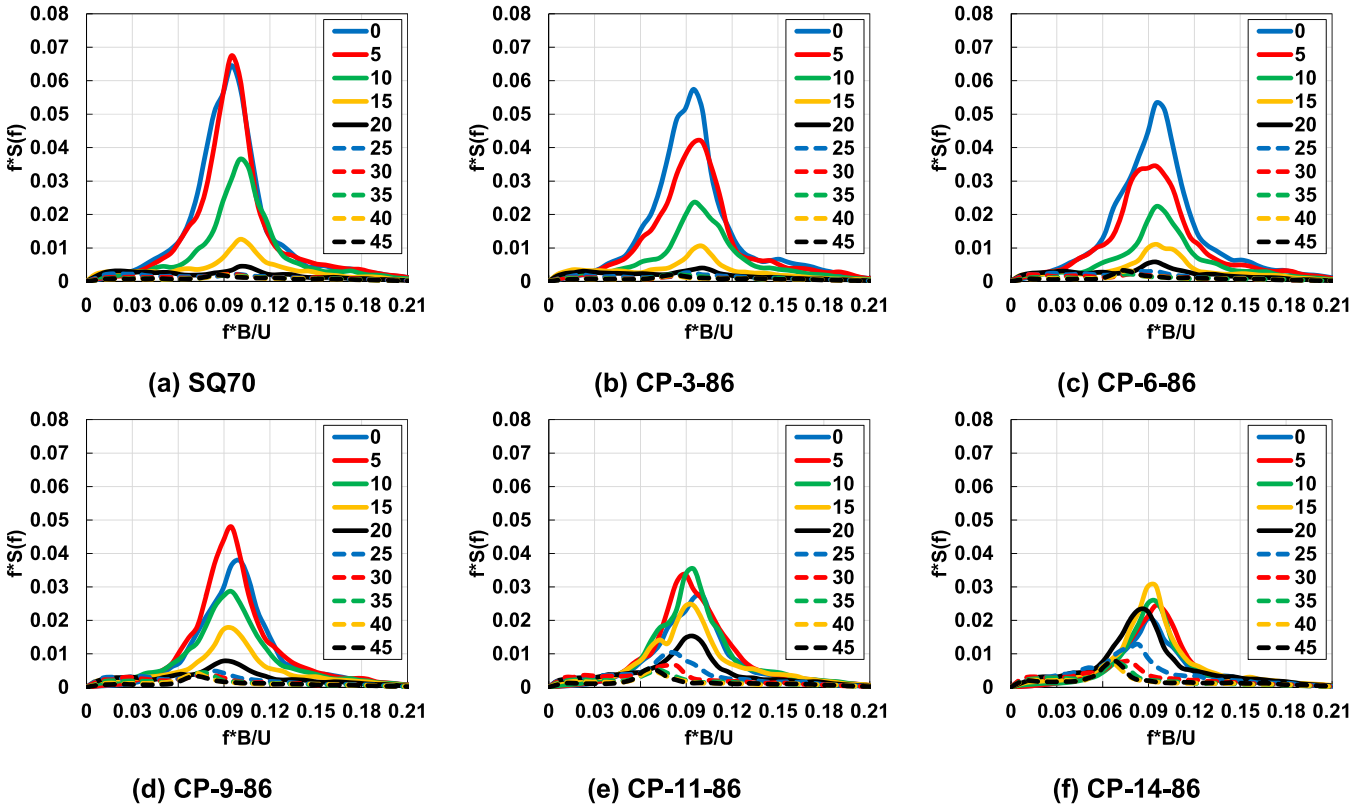

Fig. 12. Across-wind PSD responses for models with various protrusion ratios (PRs) under different wind angles.

In addition to the peak value, the PSD responses are not dominated by the same wind angle at different reduced frequencies for the corner protrusion strategy. For example, CP-14–86 is dominated by the wind angle of 20° for reduced frequencies smaller than 0.08, and controlled by the wind angle of 5° for reduced frequencies of 0.1 to 0.12. This indicates the need to analyze the results for all possible wind angles to achieve a conservative MWFRS design of high-rise buildings. On the other hand, although the dominated resonant components at different reduced frequencies can be significantly reduced using the corner protrusion strategy, the responses for wind angles larger than 20° are substantially increased (see Fig. 12(e) and (f)) in comparison with the benchmark model (see Fig. 12(a)) as a tradeoff, which is consistent with the time domain results of σ_{CML}. As discussed above, the flow behavior for the corner protrusion strategy is significantly changed for different PRs even under the same wind angle.

4.3. Structural responses for MWFRS under different design wind speeds

This section discusses the full-scale OTM responses for the ten models under different design wind speeds. Due to the negligible resonant component in the along-wind direction (see Fig. 10), the OTM responses are all dominated by the across-wind direction.

4.3.1. MWFRS design for tall buildings

After looking at the various contributing components in the above sections, Fig. 13 shows the full-scale peak OTM responses (calculated using Eq. 2) for SQ70 in the along-wind and across-wind directions for wind speeds of 25 m/s to 85 m/s. The peak OTM responses in across-wind are significantly larger than that of along-wind because of the resonant component results in the frequency domain. This also applies to the other aerodynamic modification models considered in this study. For across-wind responses, due to the variation of PSD at different

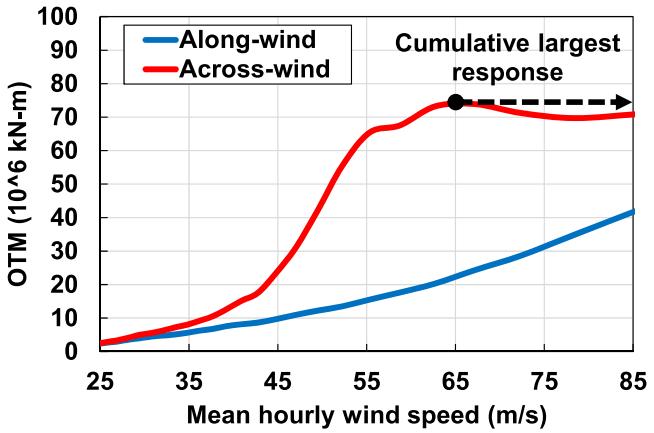

Fig. 13. Peak OTM for the benchmark model (SQ70).

reduced frequencies, the OTM responses do not increase linearly with wind speed. As shown in Fig. 13, the peak OTM in across-wind is slightly reduced when wind speeds higher than 65 m/s. This indicates that only considering a specific deign wind speed for certain performance objective (e.g., survivability) is not enough for MWFRS design. To be conservative, it is suggested to consider the cumulative largest response up to a design wind speed for the MWFRS design of high-rise buildings. For example, the OTM at 65 m/s (72×10^6 kN-m) should be used as the demand for the design wind speed of 75 m/s.

4.3.2. *Cumulative largest structural response*

The cumulative largest OTM responses for the models with various GRs are presented in Fig. 14(a), and the results normalized by the benchmark model are plotted in Fig. 14(b). By considering the cumulative largest response, the OTM responses presented in Fig. 14(a) do not decrease as wind speed increases. The design wind speeds of 1700-year return period [1] at San Francisco (SF), New York (NY), Houston (HOU), and Miami (MIA) are labeled in the figures to represent different levels of demands for survivability design in the US. The corresponding mean hourly design wind speeds at building roof are 42 m/s, 53 m/s, 62 m/s, 77 m/s, respectively.

In Fig. 14, the peak OTM responses for CP-14–0 are smaller than that of the benchmark model throughout the wind speeds considered (25 m/s to 80 m/s). This is resulted mainly from the mitigation of the background (Fig. 7(b)), and resonant (Fig. 10(b)) components in the across-wind direction. The reductions of OTM for CP-14–0 at the design wind speeds of SF, NY, HOU, and MIA are 23%, 40%, 40%, and 24%, respectively. This confirms the effectiveness of the additive side protrusion to achieve better aerodynamic performance for MWFRS under a broad range of design wind speeds. In addition, the variation of the reductions for OTM at different wind speeds suggests that only considering aerodynamic coefficients in the time domain is not enough to evaluate the performance of various aerodynamic strategies for tall buildings.

On the other hand, it can be observed that the influence of GR on the peak OTM is not significant. This demonstrates the feasibility of using the corner protrusion strategy to achieve the similar performance of the side protrusion strategy. The reductions of OTM for CP-14–86 (the model with the largest GR) at the design wind speeds of SF, NY, HOU, and MIA are 33%, 39%, 33%, and 24%, respectively, which are comparable to those of the CP-14–0. This shows the corner protrusion strategy can be produced via NCs.

The original cumulative largest OTM and normalized OTM for the models with various PRs are presented in Fig. 15. The results suggest that the performance of the corner protrusion strategy is reduced when PR decreases. The normalized peak OTM for CP-11–86 at SF, NY, HOU, and MIA are 19%, 33%, 22%, and 19%, respectively. For CP-9–86, the results are 3%, 20%, 15%, 15%, respectively. When the PR is smaller than 6%, the effectiveness to suppress wind responses disappears. Furthermore, CP-3–86 and CP-6–86 produce larger OTM than that of SQ70 at wind speeds lower than 45 m/s and higher than 75 m/s. The reason for this is attributed to the larger resonant responses at the corresponding reduced frequencies (see Fig. 11(b)). The results indicate that a PR larger than 6% is needed for the corner protrusion strategy to benefit the design of MWFRS for high-rise buildings.

4.4. *Discussion*

This study demonstrates the effectiveness of using the corner protrusion strategy to mitigate wind responses for tall buildings under various wind speeds. The results show that promising aerodynamic performance achieved from traditional aerodynamic strategy (CP-14–0) can be reproduced with various GRs (CP-14–14, CP-14–43, CP-14–71, and CP-14–86). This gives designers more freedom to pursue other design objectives, such as floor area, operation purposes, and aesthetics. For the last item, it is worth mentioning that a corner protrusion is not a rare external shape for tall buildings (i.e., the Empire State Building and the Taipei Nan Shan Plaza) in the real-world, which supports the feasibility and practicality of using the strategy to mitigate wind responses.

The need to conduct wind mitigation for high-rise buildings is well recognized in the community of wind engineering. However, this task is decoupled from the early design stage of high-rise buildings for current design practice in the industry [36]. Any changes on building shape or structural properties later in the design stage can be very expensive, time consuming, or even impossible, since floor area and structural responses are influenced at the same time. The results for models with 86% GR indicate the feasibility of using NCs to achieve the corner protrusion

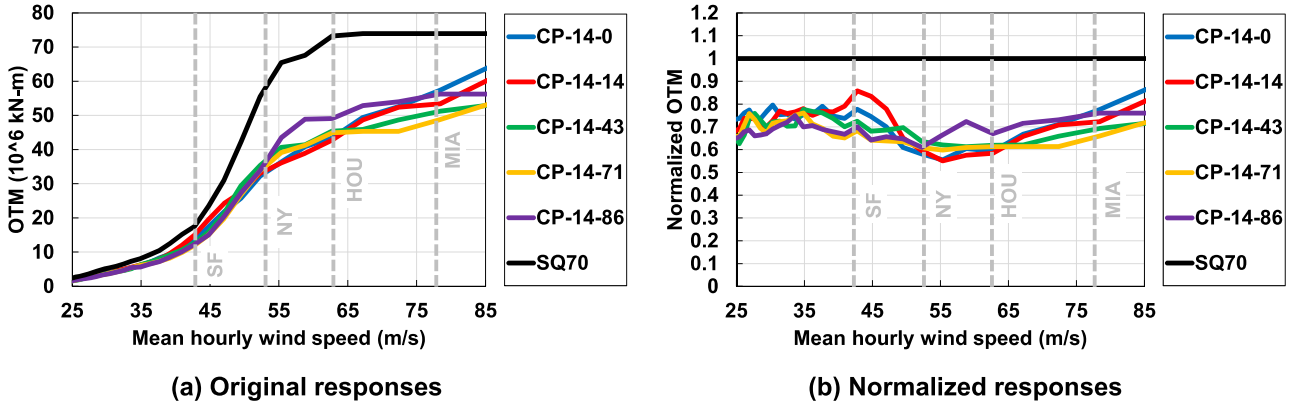

Fig. 14. Cumulative largest OTM for models with various gap ratios (GRs).

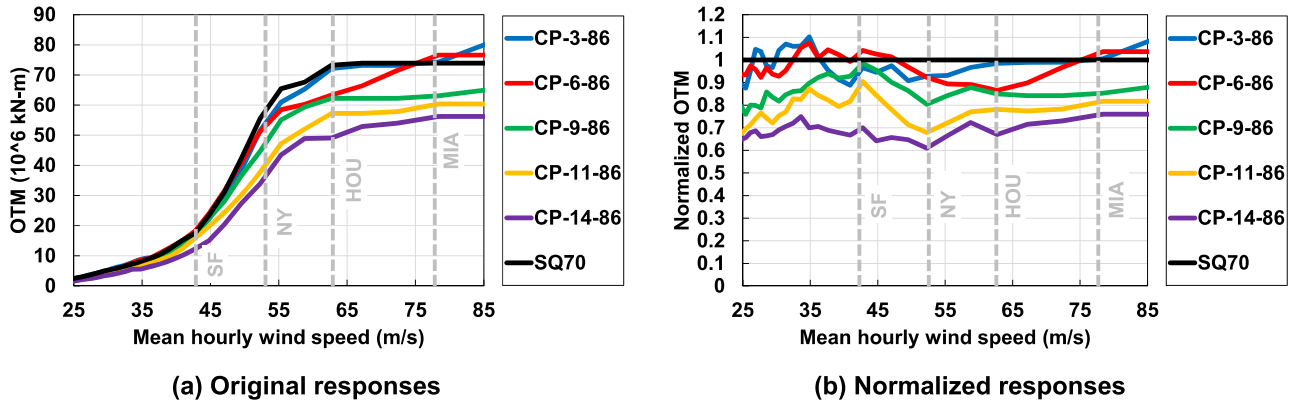

Fig. 15. Cumulative largest OTM for models with various protrusion ratios (PRs).

strategy for a later-stage modification. By applying NCs, the structural properties of the building can be preserved as the mass and the stiffness of the NCs are typically negligible in design. This indicates that the trends obtained from the OTM responses can be directly applied to the other structural responses (e.g., roof drift or acceleration) of interest. The corner protrusion strategy using NCs can simplify the design process if there are multiple strategies to compare and different objectives to pursue, which is another promising alternative for designers. In addition, the original floor area is maintained, relieving the dilemma of traditional aerodynamic strategies mentioned above.

In addition to designing a new building, the corner protrusion strategy using NCs could also provide a potential solution for aerodynamic retrofit of an existing building. The reasons for the retrofit can be (1) the deterioration of structural components, (2) the update of wind provisions, or (3) the change of approach flow conditions. Regarding the last item, it is well recognized that the aerodynamic performance of tall buildings is significantly influenced by proximity buildings due to the interference effect. The aerodynamic coefficients for an existing building could be amplified up to 50% if a new building is built in the oblique upwind direction [16,33,47,51,54]. By changing the external shape using NCs, the demands of the MWFRS could be decreased without retrofitting the structural components or adding damping inside the building. This is expected to be a competitive alternative since the influence during retrofitting (e.g., downtime) and after retrofitting (e.g., operation space) is significantly reduced.

5. Conclusions

This study investigates the effectiveness of the corner protrusion strategy with the aim of using NCs (nonstructural components) to mitigate the design demands of MWFRS (main wind force resisting system) for tall buildings over a broad range of design wind speeds. Two parameters, GR (gap ratio) and PR (protrusion ratio), are used to evaluate the various configurations for the corner protrusion strategy. HFFB (High-frequency force balanced) wind tunnel testing was conducted at the University of Florida to examine the wind performance of ten models under different wind angles. The aerodynamic coefficients in the time domain and PSD responses in the frequency domain are used to generate the base overturning moment (OTM) for the ten models. Due to the variation of PSD responses at various reduced frequencies, it is suggested to consider the cumulative largest responses for MWFRS design at different wind speeds. The following conclusions can be drawn based on the results obtained in this study:

(1) The effectiveness of additive side protrusion strategy (CP-14-0) to mitigate wind responses is confirmed. The reductions of OTM for CP-14-0 at the wind speeds of survivability design for San Francisco (42 m/s), New York (53 m/s), Houston (62 m/s), and Miami (77 m/s) are 23%, 40%, 40%, and 24%, respectively, in comparison with a square benchmark model (SQ70).
(2) The indentation in the side protrusion strategy for the design of MWFRS is negligible, suggesting that that the ideal aerodynamic performance can be produced via various GRs for the corner protrusion strategy with the same PR.
(3) The feasibility of using NCs to achieve the corner protrusion strategy is demonstrated through the models with 86% GR. The effectiveness of the corner protrusion strategy decreases with a smaller PR. To generate promising performance, the PR needs to be larger than 6%.

The aerodynamic strategy achieved via NCs is considered as a competitive solution in comparison with traditional modification strategies. Due to the boundary layer effect, the wind speed and turbulence intensity are expected to be different at various elevations. It is worthwhile to systematically investigate the optimal configurations of NCs for different approach flow conditions to mitigate the aerodynamic performance of the MWFRS with the aims of designing a new building or retrofitting an existing building.

CRediT authorship contribution statement

Wei-Ting Lu: Writing – original draft, Visualization, Validation, Methodology, Investigation, Data curation, Conceptualization. **Brian Phillips:** Writing – review & editing, Validation, Supervision, Project administration, Methodology, Conceptualization. **Zhaoshuo Jiang:** Writing – review & editing, Project administration, Conceptualization.

Declaration of Competing Interest

The authors declare that they have no known competing financial interests or personal relationships that could have appeared to influence the work reported in this paper.

Data availability

Data will be made available on request.

Acknowledgments

This material is based upon work supported by the National Science Foundation (NSF) under Grants No. 2028762 & 2028647. Any opinions, findings, and conclusions or recommendations expressed in this material are those of the authors and do not necessarily reflect the views of NSF. The authors also acknowledge the NSF NHERI awardee that contributed to the research results reported within this paper under Grant No. 2037725: Natural Hazards Engineering Research Infrastructure:

Experimental Facility with Boundary Layer Wind Tunnel 2021-2025 and Grant No. 2022469: Natural Hazards Engineering Research Infrastructure: Cyberinfrastructure (DesignSafe) 2020-2025.

References

[1] ASCE 7-22. Minimum design loads and associated criteria for buildings and other structures. Reston, VA: American Society of Civil Engineers; 2022.
[2] Carassale L, Freda A, Marre-Brunenghi M. Experimental investigation on the aerodynamic behavior of square cylinders with rounded corners. J Fluids Struct 2014;44:195–204.
[3] Catarelli RA, Fernández-Cabán PL, Masters FJ, Bridge JA, Gurley KR, Matyas CJ. Automated terrain generation for precise atmospheric boundary layer simulation in the wind tunnel. J Wind Eng Ind Aerodyn 2020;207:104276.
[4] Catarelli RA, Fernández-Cabán PL, Phillips BM, Bridge JA, Masters FJ, Gurley KR, et al. Automation and new capabilities in the University of Florida NHERI boundary layer wind tunnel. Front Built Environ 2020;6.
[5] Chen FB, Liu HM, Chen W, Shu ZR, Li Y, Li QS, et al. Characterizing wind pressure on CAARC standard tall building with various façade appurtenances: an experimental study. J Build Eng 2022;59:105015.
[6] Chen Z, Huang H, Xu Y, Tse KT, Kim B, Wang Y. Unsteady aerodynamics on a tapered prism under forced excitation. Eng Struct 2021;240:112387.
[7] Cheng X, Huang G, Yang Q, Zhou X. Influence of architectural facades on wind pressures and aerodynamic forces of tall buildings. J Struct Eng 2021;147(1):04020303.
[8] Griffis LG. Serviceability limit states under wind load. Eng J AISC 1993;1st Qtr:1–16.
[9] Gu M, Quan Y. Across-wind loads of typical tall buildings. J Wind Eng Ind Aerodyn 2004;92(13):1147–65.
[10] Gu M, Wang X, Quan Y. Wind tunnel test study on effects of chamfered corners on the aerodynamic characteristics of 2D rectangular prisms. J Wind Eng Ind Aerodyn 2020;204:104305.
[11] Hassanli S, Hu G, Fletcher DF, Kwok KCS. Potential application of double skin façade incorporating aerodynamic modifications for wind energy harvesting. J Wind Eng Ind Aerodyn 2018;174:269–80.
[12] Hou F, Sarkar P, Alipour A. A novel mechanism - smart morphing façade system - to mitigate wind-induced vibration of tall buildings. Eng Struct 2023;275:115152.
[13] Hu G, Hassanli S, Kwok KCS, Tse KT. Wind-induced responses of a tall building with a double-skin façade system. J Wind Eng Ind Aerodyn 2017;168:91–100.
[14] Hu G, Song J, Hassanli S, Ong R, Kwok KCS. The effects of a double-skin façade on the cladding pressure around a tall building. J Wind Eng Ind Aerodyn 2019;191:239–51.
[15] Hui Y, Liu J, Wang J, Yang Q. Effects of facade rib arrangement on aerodynamic characteristics and flow structure of a square cylinder. Build Environ 2022;214:108924.
[16] Hui Y, Tamura Y, Yang Q. Analysis of interference effects on torsional moment between two high-rise buildings based on pressure and flow field measurement. J Wind Eng Ind Aerodyn 2017;164:54–68.
[17] Hui Y, Yuan K, Chen Z, Yang Q. Characteristics of aerodynamic forces on high-rise buildings with various façade appurtenances. J Wind Eng Ind Aerodyn 2019;191:76–90.
[18] Irwin PA. Wind engineering challenges of the new generation of super-tall buildings. J Wind Eng Ind Aerodyn 2009;97(7-8):328–34.
[19] Jafari M, Alipour A. Review of approaches, opportunities, and future directions for improving aerodynamics of tall buildings with smart facades. Sustain Cities Soc 2021;72:102979.
[20] Kawai H. Effect of corner modifications on aeroelastic instabilities of tall buildings. J Wind Eng Ind Aerodyn 1998;74-76:719–29.
[21] Kim Y, Kanda J. Wind pressures on tapered and set-back tall buildings. J Fluids Struct 2013;39:306–21.
[22] Kwok KCS, Wilhelm PA, Wilkie BG. Effect of edge configuration on wind-induced responses of tall buildings. Eng Struct 1988;10(2):135–40.
[23] Kwon DK, Kijewski T, Kareem A. E-analysis of high-rise buildings subjected to wind loads. J Struct Eng 2008;134(7):1139–53.
[24] Li Y, Li C, Li QS, Song Q, Huang X, Li YG. Aerodynamic performance of CAARC standard tall building model by various corner chamfers. J Wind Eng Ind Aerodyn 2020;202:104197.
[25] Li Y, Song Q, Li C, Huang X, Zhang Y. Reduction of wind loads on rectangular tall buildings with different taper ratios. J Build Eng 2022;45:103588.
[26] Li YG, Yan JH, Li Y, Xiao CX, Ma JX. Wind tunnel study of wind effects on 90° helical and square tall buildings: A comparative study. J Build Eng 2021;42:103068.
[27] Liu J, Hui Y, Li S, Jiang Y. Numerical studies on aerodynamic forces and flow control regimes of square cylinder with four surface ribs. Comput Fluids 2022;245:105609.
[28] Liu J, Hui Y, Wang J, Yang Q. LES study of windward-face-mounted-ribs' effects on flow fields and aerodynamic forces on a square cylinder. Build Environ 2021;200:107950.
[29] Liu J, Hui Y, Yang Q, Tamura Y. Flow field investigation for aerodynamic effects of surface mounted ribs on square-sectioned high-rise buildings. J Wind Eng Ind Aerodyn 2021;211:104551.
[30] Liu J, Hui Y, Yang Q, Wang J. Numerical study of impact of façade ribs on the wind field and wind force of high-rise building under atmospheric boundary layer flow. J Wind Eng Ind Aerodyn 2023;236:105399.
[31] Liu J, Hui Y, Yang Q, Zhang R. LES evaluation of the aerodynamic characteristics of high-rise building with horizontal ribs under atmospheric boundary layer flow. J Build Eng 2023;71:106487.
[32] Lu WT, Phillips BM, Jiang Z. Effects of side and corner modification on the aerodynamic behavior of high-rise buildings considering serviceability and survivability. J Wind Eng Ind Aerodyn 2023;233:105324.
[33] Mara TG, Terry BK, Ho TCE, Isyumov N. Aerodynamic and peak response interference factors for an upstream square building of identical height. J Wind Eng Ind Aerodyn 2014;133:200–10.
[34] Matour S, Garcia-Hansen V, Omrani S, Hassanli S, Drogemuller R. Wind-driven ventilation of double skin façades with vertical openings: Effects of opening configurations. Build Environ 2021;196:107804.
[35] Mooneghi MA, Kargarmoakhar R. Aerodynamic mitigation and shape optimization of buildings: review. J Build Eng 2016;6:225–35.
[36] Moorjani RR, Lombardo FT, Devin AF, Young BS, Baker WF, Ray SD. Influence of vented floors on the across-wind response of tall buildings. J Wind Eng Ind Aerodyn 2021;209:104480.
[37] Quan Y, Kuang J, Gu M, Wang S. Effects of grid curtains on the wind loads of a high-rise building. Struct Des Tall Spec Build 2016;25:245–62.
[38] Shameri MA, Alghoul MA, Sopian K, Zain MFM, Elayeb O. Perspectives of double skin façade systems in buildings and energy saving. Renew Sustain Energy Rev 2011;15:1468–75.
[39] Sharma A, Mittal H, Gairola A. Mitigation of wind load on tall buildings through aerodynamic modifications: review. J Build Eng 2018;18:180–94.
[40] Skvorc P, Hozmar H. The effect of wind characteristics on tall buildings with porous double-skin façades. J Build Eng 2023;69:106135.
[41] Stathopoulos S, Zhu X. Wind pressures on buildings with mullions. J Struct Eng 1990;116(8):2272–91.
[42] Stathopoulos T. Wind environmental conditions around tall buildings with chamfered corners. J Wind Eng Ind Aerodyn 1985;21:71–87.
[43] Tamura T, Miyagi T. The effect of turbulence on aerodynamic forces on a square cylinder with various corner shapes. J Wind Eng Ind Aerodyn 1999;83:135–45.
[44] Tanaka H, Tamura Y, Ohtake K, Nakai M, Kim YC. Experimental investigation of aerodynamic forces and wind pressures acting on tall buildings with various unconventional configurations. J Wind Eng Ind Aerodyn 2012;107–108:179–91.
[45] Tschanz T, Davenport AG. The base balance technique for the determination of dynamic wind loads. J Wind Eng Ind Aerodyn 1983;13(1-3):429–39.
[46] Tse KT, Hitchcock PA, Kwok KC, Thepmongkorn S, Chan CM. Economic perspectives of aerodynamic treatments of square tall buildings. J Wind Eng Ind Aerodyn 2009;97(9–10):455–67.
[47] Wang T, Kwok KCS, Yang Q, Tian Y, Li B. Experimental study on proximity interference induced vibration of two staggered square prisms in turbulent boundary layer flow. J Wind Eng Ind Aerodyn 2022;220:104865.
[48] Xiang C, Matusiak BS. Façade Integrated Photovoltaics design for high-rise buildings with balconies, balancing daylight, aesthetic and energy productivity performance. J Build Eng 2022;57:104950.
[49] Yang Q, Liu Z, Hui Y, Li Z. Modification of aerodynamic force characteristics on high-rise buildings with arrangement of vertical plates. J Wind Eng Ind Aerodyn 2020;200:104155.
[50] Yoon N, Min D, Heo Y. Dynamic compartmentalization of double-skin façade for an office building with single-sided ventilation. Build Environ 2022;208:108624.
[51] Yu X, Xie Z, Gu M. Interference effects between two tall buildings with different section sizes on wind-induced acceleration. J Wind Eng Ind Aerodyn 2018;182:16–26.
[52] Yuan K, Hui Y, Chen Z. Effects of facade appurtenances on the local pressure of high-rise building. J Wind Eng Ind Aerodyn 2018;178:26–37.
[53] Zhou Y, Kijewski T, Kareem A. Aerodynamic loads on tall buildings: interactive database. J Struct Eng 2003;129(3):394–404.
[54] Zu GB, Lam KM. Across-wind excitation mechanism for interference of twin tall buildings in staggered arrangement. J Wind Eng Ind Aerodyn 2018;177:167–85.